CHEMISTRY OF MATERIALS
Article

Chem. Mater. **2009,** *21,* 4955–4961 4955
DOI:10.1021/cm902199p

Controlled Growth and Magnetic Property of FePt Nanostructure: Cuboctahedron, Octapod, Truncated Cube, and Cube

Shang-Wei Chou,[†] Chun-Ling Zhu,[†] Sonnathi Neeleshwar,[‡] Cheng-Lung Chen,[‡] Yang-Yuan Chen,[‡] and Chia-Chun Chen*[,†,§]

[†]*Department of Chemistry, National Taiwan Normal University, Taipei 11677, Taiwan,* [‡]*Institute of Physics, Academia Sinica, Taipei 11529, Taiwan, and* [§]*Institute of Atomic and Molecular Sciences, Academia Sinica, Taipei 10617, Taiwan*

Received July 19, 2009. Revised Manuscript Received September 4, 2009

The strategy for shape control of alloy FePt nanocrystal was studied systematically. By the careful adjustments of reaction parameters in a solution reaction, surfactant−facet bindings on the growth seed were controlled delicately. FePt octapod, cuboctahedron, truncated cube, and nanocube were successfully prepared from cuboctahedral seed and examined by high-resolution transmission electron microscopy. The formations of FePt nanostructures were mainly attributed to the differences in the growth rate between the {111} and {100} planes of cuboctahedral seeds. The magnetic measurements showed that the order of volume, $V_{(\text{nanocube})} > V_{(\text{octapod})} > V_{(\text{cuboctahedron})}$ obviously reflected the order of saturated magnetization (M_s), $M_{s\ (\text{nanocube})} > M_{s\ (\text{octapod})} > M_{s\ (\text{cuboctahedron})}$. Furthermore, the measurements of octapod exhibited the highest coercivity and blocking temperature because of its higher surface to volume ratio and more structural facets.

Introduction

The syntheses of magnetic nanocrystals have been studied extensively due to their great potentials for magnetic resonance imaging, separation, data storage and high performance permanent magnets.[1−7] Recently, many studies have demonstrated that different types of magnetic nanocrystals such as the pure metal and metal oxide were prepared with a well-defined shape by the careful controls in solution phase reactions.[8,9] Several experimental results have revealed that the magnetic properties of the nanocrystals such as magnetocrystalline anisotropy and blocking temperature strongly correlated with their shapes.[10−12] For examples, the magnetocrystalline anisotropy of Fe nanorods was higher than that of Fe spherical nanoparticles.[10] The blocking temperature was higher for spherical particle of γ-Fe_2O_3 than for cubic shape of γ-Fe_2O_3.[11] The origin of shape dependency of their magnetic characteristics was mainly attributed to the difference of their shape and/or surface anisotropy. Besides the studies of the pure metal and metal oxide, alloy magnetic nanocrystals such as FePt, FeCo, CoPt have recently become the center of attention in this field.[4−7,13,14] However, the growth of magnetic alloy nanocrystals were much more difficult than that of pure metal nanocrystals because the controls of the sizes, shapes, compositions and even atomic ordering degree of the alloy were much complicated during the growth in the solution phase.[15] The systematically controlled growth of alloy magnetic nanocrystals was still a challenging step to overcome.

Previous reports have shown that alloy FePt nanocrystals with cubic, wirelike, and rodlike shapes (nanocubes, nanowires and nanorods) were prepared through "surfactant-assisted mechanism" in the solution reaction.[16−18] Several works on the syntheses of pure

*To whom correspondence should be addressed. E-mail: cjchen@ntnu.edu.tw.

(1) Jun, Y. W.; Seo, J. W.; Cheon, J. *Acc. Chem. Res.* **2008**, *41*, 179.
(2) Jeong, U.; Teng, X. W.; Wang, Y.; Yang, H.; Xia, Y. N. *Adv. Mater.* **2007**, *19*, 33.
(3) Yavuz, C. T.; Mayo, J. T.; Yu, W. W.; Prakash, A.; Falkner, J. C.; Yean, S.; Cong, L. L.; Shipley, H. J.; Kan, A.; Tomson, M.; Natelson, D.; Colvin, V. L. *Science* **2006**, *314*, 964.
(4) Sun, S. H.; Murray, C. B.; Weller, D.; Folks, L.; Moser, A. *Science* **2000**, *287*, 1989.
(5) Sun, S. H. *Adv. Mater.* **2006**, *18*, 393.
(6) Chaubey, G. S.; Barcena, C.; Poudyal, N.; Rong, C. B.; Gao, J. M.; Sun, S. H.; Liu, J. P. *J. Am. Chem. Soc.* **2007**, *129*, 7214.
(7) Beecher, P.; Shevchenko, E. V.; Weller, H.; Quinn, A. J.; Redmond, G. *Adv. Mater.* **2005**, *17*, 1080.
(8) Puntes, V. F.; Krishnan, K. M.; Alivisatos, A. P. *Science* **2001**, *291*, 2115.
(9) Jana, N. R.; Chen, Y. F.; Peng, X. G. *Chem. Mater.* **2004**, *16*, 3931.
(10) Park, S. J.; Kim, S.; Lee, S.; Khim, Z. G.; Char, K.; Hyeon, T. *J. Am. Chem. Soc.* **2000**, *122*, 8581.
(11) Salazar-Alvarez, G.; Qin, J.; Sepelak, V.; Bergmann, I.; Vasilakaki, M.; Trohidou, K. N.; Ardisson, J. D.; Macedo, W. A. A.; Mikhaylova, M.; Muhammed, M.; Baro, M. D.; Nogues, J. *J. Am. Chem. Soc.* **2008**, *130*, 13234.
(12) Yanes, R.; Chubykalo-Fesenko, O.; Kachkachi, H.; Garanin, D. A.; Evans, R.; Chantrell, R. W. *Phys. Rev. B* **2007**, *76*, 06441–6.
(13) Zhao, F.; Rutherford, M.; Grisham, S. Y.; Peng, X. *J. Am. Chem. Soc.* **2009**, *131*, 5350.
(14) Wang, D. Y.; Chen, C. H.; Yen, H. C.; Lin, Y. L.; Huang, P. Y.; Hwang, B. J.; Chen, C. C. *J. Am. Chem. Soc.* **2007**, *129*, 1538.
(15) Ferrando, R.; Jellinek, J.; Johnston, R. L. *Chem. Rev.* **2008**, *108*, 845–910.
(16) Chen, M.; Kim, J.; Liu, J. P.; Fan, H. Y.; Sun, S. H. *J. Am. Chem. Soc.* **2006**, *128*, 7132.
(17) Chen, M.; Pica, T.; Jiang, Y. B.; Li, P.; Yano, K.; Liu, J. P.; Datye, A. K.; Fan, H. Y. *J. Am. Chem. Soc.* **2007**, *129*, 6348.
(18) Wang, C.; Hou, Y. L.; Kim, J. M.; Sun, S. H. *Angew. Chem., Int. Ed.* **2007**, *46*, 6333.

Published on Web 09/28/2009

Table 1. Experimental Parameters and Results of the Syntheses of FePt Nanocrystals

sample no.	FePt nanocrystals (composition)	OA/OL/HDD	$Pt(acac)_2/Fe(CO)_5$	reaction time
1	octapod ($Fe_{72}Pt_{28}$)	4 mL/4 mL/1.05 g	47 mg/66 μL	60 min
2	cuboctahedron ($Fe_{72}Pt_{28}$)	6 mL/2 mL/1.05 g	47 mg/66 μL	60 min
3	nanocube ($Fe_{72}Pt_{28}$)	4 mL/4 mL/5.0 g	47 mg/66 μL	60 min
4	nanocube ($Fe_{35}Pt_{65}$)	4 mL/4 mL/1.05 g	95 mg/66 μL	60 min
5	mixture of cuboctahedron, truncated cube	4 mL/4 mL/1.05 g	47 mg/66 μL	5 s
6	mixture of octapod, filled octapod, nanocube	4 mL/4 mL/5.0 g	47 mg/66 μL	5 min

metal nanocrystals such as Au nanocubes, Pd octahedrons and Pt cuboctahedrons have also indicated that the surfactants played a key role on the shape control.[19−22] The surfactants such as oleyl amine (OLAm) and oleic acid (OA) played the major roles for the controls of resulting nanocrystal morphologies. First, surfactants might form a micelle that was treated as a soft template for the confined crystal growth.[23] Also, the precursors and surfactants might form complexes so that the crystal growth pathway was altered.[24] The formation of the complexes have been well characterized by FT-IR and NMR spectrometry recently.[13] The surfactant was served as a capping ligand as well as a reducing agent. Furthermore, the surfactants might generate strong bindings on the facets of nanocrystals during the growth. The surfactant-facet bindings usually resulted in the different growth rates of the planes, and consequentially the shapes of resulting nanocrystals were varied.[25−27] Through the adjustments of surfactant ratios in the reactions, the successful formations of cubic FeCo and PbTe nanocrystals have been achieved.[28,29] Thus, further studies on the controlled growth of alloy metal nanocrystals become important to understand detailed growth mechanism of the nanocrystals of various shapes and to explore their physical properties.

In this paper, we have developed a systematical strategy to achieve the shape controls of alloy FePt nanocrystals by the careful adjustments of reaction parameters in a solution reaction. The FePt nanocrystals with octapod, cuboctahedral, truncated cubic and cubic shapes were successfully prepared and examined by high-resolution transmission electron microscopy (HRTEM). The formation of FePt nanocrystals was mainly attributed to the differences in the growth rate between the {111} and {100} planes of cuboctahedral seeds as we proposed in the growth mechanism. Furthermore, the magnetic measurements indicated that the coercivity and blocking temperature of FePt nanocrystals exhibited remarkable shape dependencies. The FePt nanocrystals with unique shapes and magnetic characteristics might be applied for new magnetic devices.

(19) Sun, Y. G.; Xia, Y. N. *Science* **2002**, *298*, 2176.
(20) Bratlie, K. M.; Lee, H. J.; Komvopoulos, K.; Yang, P. D.; Somorjai, G. A. *Nano Lett*. **2007**, *7*, 3097.
(21) Xiong, Y. J.; Xia, Y. N. *Adv. Mater*. **2007**, *19*, 3385.
(22) Chen, J. Y.; Lim, B.; Lee, E. P.; Xia, Y. N. *Nano Today* **2009**, *4*, 81.
(23) Burda, C.; Chen, X. B.; Narayanan, R.; El-Sayed, M. A. *Chem. Rev*. **2005**, *105*, 1025.
(24) Peng, Z. A.; Peng, X. *J. Am. Chem. Soc*. **2001**, *123*, 1389.
(25) Yin, Y.; Alivisatos, A. P. *Nature* **2005**, *437*, 664.
(26) Hou, Y. L.; Xu, Z. C.; Sun, S. H. *Angew. Chem., Int. Ed*. **2007**, *46*, 6329.
(27) Jun, Y. W.; Choi, J. S.; Cheon, J. *Angew. Chem., Int. Ed*. **2006**, *45*, 3414.
(28) Wei, X. W.; Zhu, G. X.; Liu, Y. J.; Ni, Y. H.; Song, Y.; Xu, Z. *Chem. Mater*. **2008**, *20*, 6248.
(29) Mokari, T. L.; Zhang, M. J.; Yang, P. D. *J. Am. Chem. Soc*. **2007**, *129*, 9864.

Experimental Section

Synthesis of FePt Nanocrystals. Platinum acetylacetonate ($Pt(acac)_2$, ACROS, 97%), iron pentacarbonyl ($Fe(CO)_5$, Aldrich, 99.99%), hexadecane-1,2-diol (HDD, Aldrich, 90%), dioctyl ether (Aldrich, 90%), oleyl amine (OLAm, Aldrich, 70%), and oleic acid (OA, Aldrich, 90%) were used as received. $Pt(acac)_2$, $Fe(CO)_5$, OA, OLAm, and HDD were mixed with dioctyl ether (4 mL) under N_2. The mixture was heated at 240 °C for certain periods (5 s to 60 min.) and then cooled to the room temperature gradually. The final product was precipitated by adding ethanol and methanol into the mixture and then separated by centrifugation for further characterization. The experimental parameters and results of the syntheses of FePt nanocrystals were summarized in Table 1.

Characterization. A JEOL JSM-1200EX II and Philips/FEI Tecnai 20 G2 S-Twin transmission electron microscopes were used for the structural analyses at an accelerating voltage of 200 kV. A small amount of sample was deposited on an amorphous carbon membrane supported by a copper grid. The size and morphology were determined at magnification of 200k, 300k and 450k. The powder X-ray diffraction was executed on a Bruker D8 Advance diffractometer. The FePt powder was placed on silicon wafer and the workup procedure was carried out with Cu $K\alpha$ radiation (λ = 1.54178 Å). The compositional analysis was performed using Jobin-Yvon emission, JY-24 inductively coupled plasma atomic emission spectroscopy (ICP-AES). Magnetic measurements were carried out using commercial SQUID (superconducting quantum interference device) magnetometer (MPMS, Quantum Design). FePt samples (10−20 mg) were loaded into tube and the measurements were recorded between −30 000 and 30 000 Oe at room temperature. The measurements of blocking temperature were recorded between 5 and 300 K at the fixed magnetic field ~100 Oe.

Results and Discussion

The reaction of $Pt(acac)_2$ and $Fe(CO)_5$ were performed to prepare FePt nanocrystals in the presence of the surfactants, OA and OLAm. The reaction parameters including the ratios of surfactants and precursors, and also reaction time were adjusted to control the size and shape of resulting FePt nanocrystals. The results are presented respectively in the followings. Figure 1A shows the products were prepared at the OA/OLAm (v/v) = 1/1 and the fixed concentration of the reactants. The nanocrystals with an unusual shape were found in the image. The length of the nanocrystals in the projected image referred to the distance of one side to its opposite side is approximately 12.18 ± 0.3 nm. The resulting

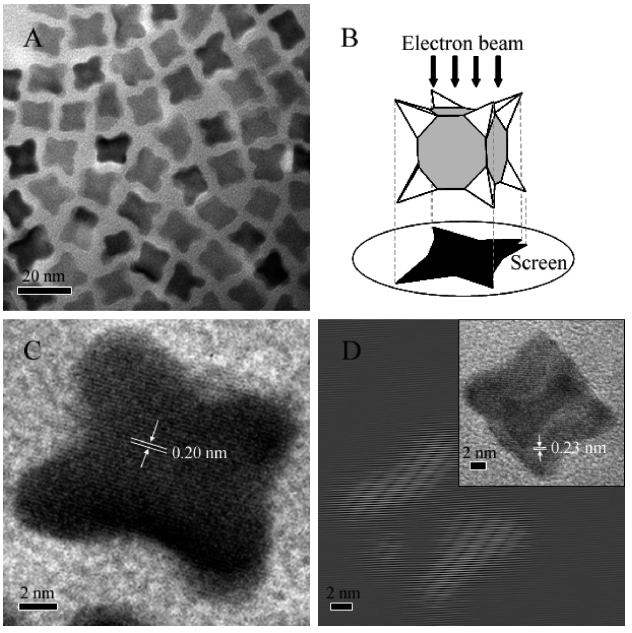

Figure 1. (A) TEM image of octapods. (B) The schematic illustration of the projection of a three-dimensional octapod structure under an electron beam. The white and gray colors represent the {111} and {100} facets of the octapod (top), respectively. (C) High-resolution TEM image of an octapod. (D) The analysis of FFT and HRTEM image of an octapod after tilting the sample holder for 25°. In the analysis of FFT, the {111} facets (the gray area) were distributed primarily over the angular corners.

nanocrystals with elongated corners and symmetrical pods are observed obviously. To clearly identify the shape of the nanocrystals, Figure 1B demonstrates the schematic illustration of the projection of a three-dimensional "octapod" structure under an electron beam.[30] The projection image suggests that the resulting products of nanocrystals in Figure 1A are the octapod structure that the nanocrystals with eight tetrahedron on the corners along the [111] directions of a truncated cubic-based structure. Here, the nanocrystals with the octapod shape as shown in Figure 1B are called as octapod. The high-resolution TEM image (HRTEM) in Figure 1C indicates that the distance between adjacent lattice fringes is ~0.20 nm. The interplanar distance is close to the lattice spacing of the (200) facet of FePt alloy (0.192 nm, JCPDS card no. 02−1167). After tilting the sample holder 25°, the HRTEM image shows that the lattice distance is 0.23 nm as illustrated in the inset of Figure 1D. The lattice distance is close to that of the (111) facet (0.232 nm, JCPDS card no. 02−1167). Through the analysis of fast Fourier transformation (Figure 1D), the {111} facets (the gray area) were distributed primarily over the angular corners. Besides the TEM measurements, FePt nanocrystals in this work were also characterized by inductively coupled plasma atomic emission spectroscopy (ICP-AES). The composition of FePt octapod was Fe/Pt = 72/28 based on ICP-AES measurements when the molar ratio of $Fe(CO)_5/Pt(acac)_2$ = 4/1 was used.

The increases in the ratios of OA/OLAm were performed to further understand the morphology change of

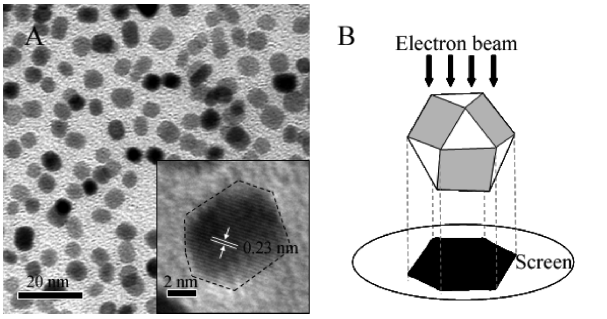

Figure 2. (A) TEM image of cuboctahedrons. The HRTEM image (inset) of cuboctahedron exhibits a clear hexagonal projection as guided by a dash line. (B) The schematic drawing of the projection of a three-dimensional "cuboctahedron" structure under an electron beam. The white and gray colors represent the {111} and {100} facets, respectively.

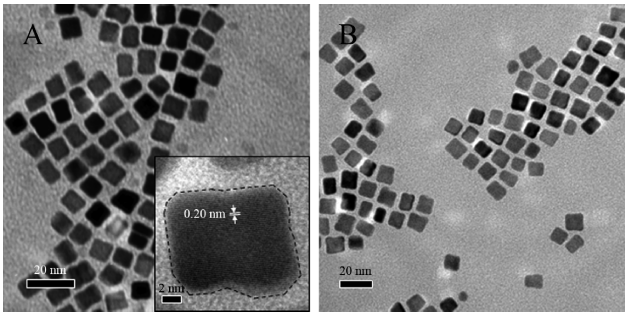

Figure 3. (A) TEM image of nanocubes synthesized in the HDD-rich condition (sample 3). The HRTEM image shows that the cube with irregular edges (indicated by dash line) is enclosed by (200) plane. (B) TEM image of nanocubes prepared in the relatively Pt-rich condition (sample 4).

resulting nanocrystals. Figure 2A shows the TEM images of the FePt nanocrystals when OA/OLAm was 3/1 used in the reaction (in comparison to OA/OLAm = 1/1 used for the sample in Figure 1). The nanocrystals exhibited a faceted structure with uniform size. On average, the diameter of the nanocrystals is 6.8 ± 0.7 nm and their size distribution was quite uniform. The hexagonal shape is clearly observed in the HRTEM image. The spacing between adjacent lattice fringes is ~0.23 nm. The interplanar distance is close to the lattice spacing of the (111) facet of FePt alloy (0.232 nm, JCPDS card no. 02−1167). To clear identify the shape of the nanocrystals, Figure 2B shows the schematic illustration of the projection of a three-dimensional "cuboctahedral" structure under an electron beam. The cuboctahedral structure matches the hexagonal projection observed in the TEM image of Figure 2A. As we compared the results in Figure 1, we found that FePt nanocrystals with cuboctahedral shapes were obtained only by the increases of the ratio of OA/OLAm in the solution reaction. In addition, the ICP-AES measurements demonstrated that the alloying composition of FePt cuboctahedron was Fe/Pt = 72/28.

The concentration of hexadecane-1,2-diol (HDD) was increased to 5 times for the study of effect on resulting shapes of FePt nanocrystals (in comparison to the [HDD] used for the sample in Figure 1). The TEM images in Figure 3A shows that the structure of resulting nanocrystals was mainly cubic shape (nanocubes). Their size

(30) Ren, J. T.; Tilley, R. D. *J. Am. Chem. Soc.* **2007**, *129*, 3287.

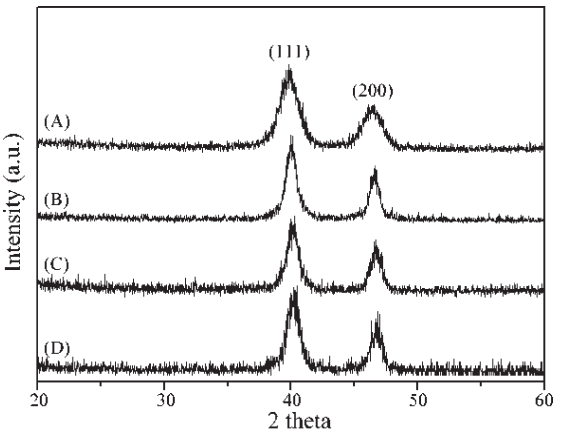

Figure 4. XRD patterns of (A) cuboctahedron (sample 2), (B) octapod (sample 1), (C) nanocube prepared in HDD-rich condition (sample 3), and (D) nanocube synthesized in relatively Pt-rich condition (sample 4).

distribution referred to the lengths of one side in the projected images is 11.8 ± 1.0 nm. The HRTEM image in the inset of Figure 3A shows the lattice spacing (0.20 nm) was close to the interplanar distance of FePt (200) facet. The TEM results displayed that the cubic FePt nanocrystal was enclosed mainly by the (200) facet, particularly, the nanocubes exhibited "not-sharp" and irregular edges but not the edges as a perfect cube. Likewise, a large amount of FePt nanocubes was observed under TEM (Figure 3B) when precursor ratio was changed to $Fe(CO)_5/Pt(acac)_2$ = 2/1 (in comparison to $Fe(CO)_5/Pt(acac)_2$ = 4/1 used for the sample in Figure 1). The average size (12.0 ± 0.8 nm) and morphology of the cubes in this case (Figure 3B) was similar to that of nanocubes as shown in Figure 3A. However, the composition of FePt nanocubes was changed when the ratios of the precursors were varied. The alloying compositions of nanocubes under those two synthetic parameters were found to be Fe/Pt = 72/28 (Figure 3A) and Fe/Pt = 35/65 (Figure 3B), respectively. Besides the TEM measurements, the typical XRD patterns of FePt nanocrystals were shown in Figure 4. Two strong peaks of (111) and (200) of a FCC structure in all four samples were clearly observed. The shift ($\Delta 2\theta \approx 0.2$) of (111) and (200) peaks of nanocubes away from those of other three samples might be mainly due to the differences of their alloy compositions, which was also confirmed by the ICP-AES measurements.[31] Also, the particle sizes of the sample calculated based on Scherrer's equation were consistent with the data obtained from TEM measurements.[32]

The FePt nanocrystals were also successfully collected even though the reaction was completed under a very short reaction time (5 s relative to 1 h in the synthetic condition of FePt octapods in Figure 1). The results provided interesting information for the studies of shape evolutions during the crystal growth. The FePt nanocrystals with cuboctahedral and truncated cubic shapes (Figure 5A) were both observed for the reaction in 5 s. Figure 5B are representative HRTEM images of cuboctahedral and truncated cubic shapes, and shows the lattice spacing of (111) and (200) planes, respectively. The average size based on the diameter of cuboctahedral shape is 5.3 ± 0.8 nm. Also, the average size referred to the lengths of one side in the projected image of FePt truncated cubes is 8.1 ± 0.7 nm. Particularly, the truncated cubic nanocrystals exhibited regular faceted edges. On the basis of the size difference between truncated cubes and cuboctahedral particles in Figure 5A, we suggested that the former were grown from the later when the growth rate of {111} plane was higher than that of {100} plane (Figure 5C).[33] However, when the total reaction became 5 min (in comparison to 60 min applied for the sample in Figure 3A), the resulting products showed both FePt nanocube and octapod as observed in TEM image (Figure 5D). The average sizes of the octapods and nanocubes here (see Figure 1A and 3B for the definitions of the sizes) are 12.0 ± 1.2 and 12.0 ± 0.6 nm, respectively. Figure 5E shows the HRTEM image of octapod and filled octapod. Also, the HRTEM image showed the filled octapod is enclosed by (200) plane and the lattice distance is ~0.20 nm. On the basis of the information obtained in images D and E in Figure 5, we believed that the nanocubes were evolved from the octapods by the rapid growth of {100} planes to form "filled octapods" (Figure 5F). Here, the filled octapods were treated as a transition structure between FePt octapods and nanocubes. Importantly, when the total reaction time was extended to be 60 min, the results showed that only cubes were obtained. Under a thermodynamically controlled growth trend, the nanocubes were expected to be the most stable structure of a face-centered cubic (FCC) crystal.[34]

The shape evolutions of FePt nanocrystals during the crystal growth were proposed and described by pathways A−D in Figure 6 based on our experimental results. At the beginning of the growth, Fe and Pt atoms started to form cuboctahedral seeds. In a cuboctahedral seed, there were 8 {111} facets and 6 {100} facets with the minimum of the total surface energy.[35] The nanocrystals with various shapes were developed from the seed depending on their reaction conditions. In pathway A, the cuboctahedral seed evolved into a truncated cube when the growth rate of the {111} plane ($G\{111\}$) was relatively higher than that of the {100} plane ($G\{100\}$). Here, the growth rates were mainly controlled by the adjustments of the types and concentrations of surfactants. However, when the $G\{111\}$ was far much higher than the $G\{100\}$ during the growth, cuboctahedral seed was evolved into octapod (Pathway B).[30] On the other hand, when the $G\{111\}$ was almost equal to the $G\{100\}$, cuboctahedron with the size larger than that of the seed were obtained (pathway C). According to our experimental results, one

(31) Klemmer, T. J.; Shukla, N.; Liu, C.; Wu, X. W.; Svedberg, E. B.; Mryasov, O.; Chantrell, R. W.; Weller, D. *Appl. Phys. Lett.* **2002**, *81*, 2220.
(32) Klug, H. P.; Alexander, L. E. *X-ray Diffraction Procedures for Polycrystalline and Amorphous Materials*; Wiley: New York, 1962.
(33) Wang, Z. L. *J. Phys. Chem. B* **2000**, *104*, 1153.
(34) Ahmadi, T. S.; Wang, Z. L.; Henglein, A.; ElSayed, M. A. *Chem. Mater.* **1996**, *8*, 1161.
(35) Wulff, G.; Kristallogr, Z.; **1901**, *34*, 449.

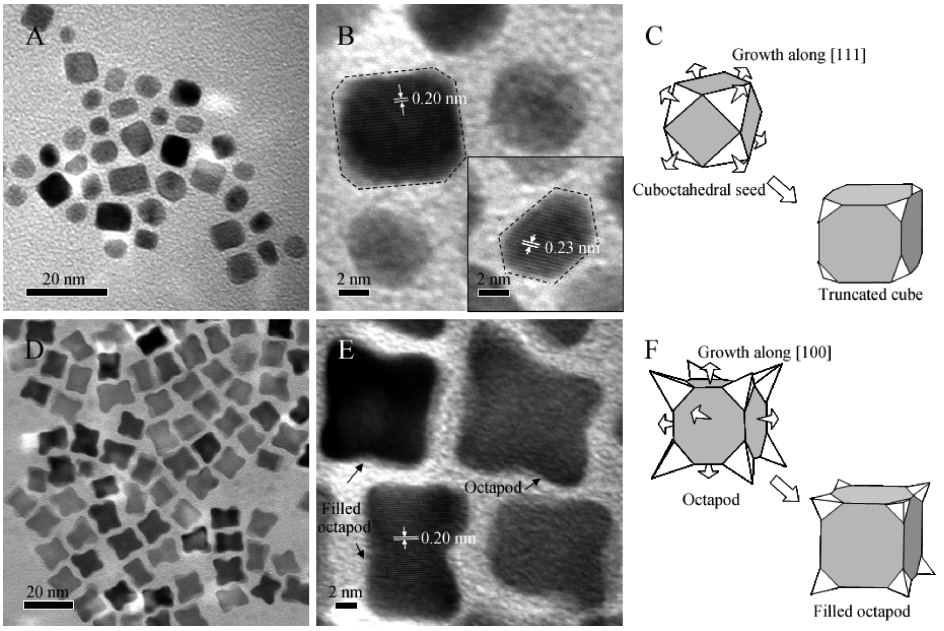

Figure 5. (A) TEM image of the mixture of FePt nanocrystals with cuboctahedral seeds and truncated cubes (B) The HRTEM image of cuboctahedral and truncated cubic shape (guided by a dash line). (C) The graphic representation of a three-dimensional cuboctahedral seed transform into truncated cube through the growth along the [111] directions. The white and gray colors represent the {111} and {100} facets, respectively. (D) TEM image of the mixture of octapods, filled octapods, and nanocubes. (E) The HRTEM image of octapod and filled octapod. (F) The graphic representation of a three-dimensional octapod grew into filled octapod through the growth along the [100] directions. The white and gray colors represent the {111} and {100} facets, respectively.

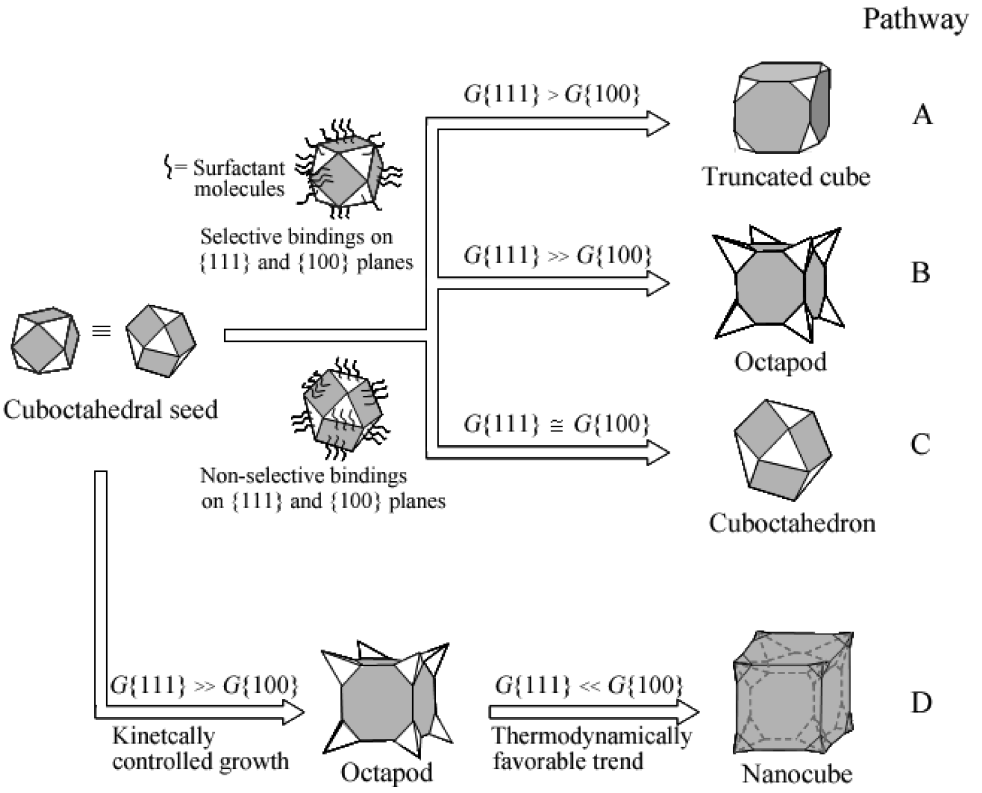

Figure 6. Schematic illustration of the formations of truncated cube (pathway A), octapod (pathway B), cuboctahedron (pathway C), and nanocube (pathway D). All the nanocrystals were formed originally from the cuboctahedral seeds (left). The white and gray colors represent the {111} and {100} facets of the FePt nanocrystals, respectively.

of the key factors to determine the reaction going through pathway A, B, or C was the adjustments of the ratio of OA and OLAm concentrations. When the ratio was varied, the $G\{111\}$ and $G\{100\}$ were changed significantly because there were strong "surfactant−facet bindings" between the surfactant molecule and crystal surfaces.

Several previous reports have pointed out that "surfactant-facet binding" was a key factor for the control of the kinetic and thermodynamic parameters in the syntheses of metal nanocrystals such as Au and Ag nanocubes, Pd octahedrons, and Pt cuboctahedron.[19−22,36] In our works, the amine group of OLAm generated stronger surfactant-facet bindings on {100} planes than on {111} planes. On the other hand, OA generated equal surfactant−facet bindings on both planes. Surface energies of {111} and {100} planes were decreased differently by these surfactant-facet bindings when the different amounts of OLAm and OA were bound onto {111} and {100} planes. Because the growth rate of crystal facets was proportional to the surface energy of crystal facets, the $G\{111\}$ was much higher than $G\{100\}$ in the reaction when [OLAm] was increased (pathway B). On the other hand, the $G\{111\}$ and $G\{100\}$ were comparable when the [OA] were increased (pathway C).

In pathway D of Figure 6, the nanocubes were eventually formed. In our experiments, the cubic shape was prepared under two different pathways. First, the cubes (or truncated cubes) were formed when the $G\{111\}$ was higher than $G\{100\}$ in FCC crystals (pathway A). However, Pathway D described an alternative pathway for the formation of the cubic shape. At the beginning of growth, $G\{111\}$ of cuboctahedral seed was far much higher than $G\{100\}$ of cuboctahedral seed and then the octopad were formed. Afterward, the growth rate was reversed ($G\{100\} \gg G\{111\}$). The areas along [100] directions were filled rapidly. Eventually, the nanocubes were formed if the reaction time was extended to be long enough. On the basis of our experimental results, the formation of FePt octapods at the first step was achieved under the conditions that the [OLAm]/[OA] were relatively high. At the beginning of growth, the octapods were quickly formed from cuboctahedral seeds within a short time under the high concentrations of the metal atoms in solution. At this stage, the growth was driven by a kinetically controlled trend ($G\{111\} \gg G\{100\}$) because of specific surfactant-facet bindings. Then, the metal atom concentrations dropped significantly after the formation of octapods. Therefore, the reaction turned out to be a thermodynamically controlled growth at the second step in the case of low concentrations of metal atoms left still in the solution. Similar to the ripening process of nanocrystals, the metal atoms tend to deposit on the low energy facets, the {100} planes of octapod.[11,24,37] Eventually, FePt nanocubes, the thermodynamically favorable products, were obtained. The similar two-step mechanism has been proposed previously in the preparation of Pt nanocubes and octapods.[30] The growth of Pt nanocubes was explained by the formation of Pt octapods at the first stage followed by, the filling along the [100] directions of Pt octapods. It was energetically favorable for enclosure by the {100} facets and eventually the nanocubes were formed. Overall, our proposed pathways in Figure 6 were able to explain successfully the formation of truncated cubes, octapods, cuboctahedrons, and nanocubes. Thus, the reaction pathway in the growth was controlled by careful adjustments of reaction parameters in the growth of FePt nanocrystals.

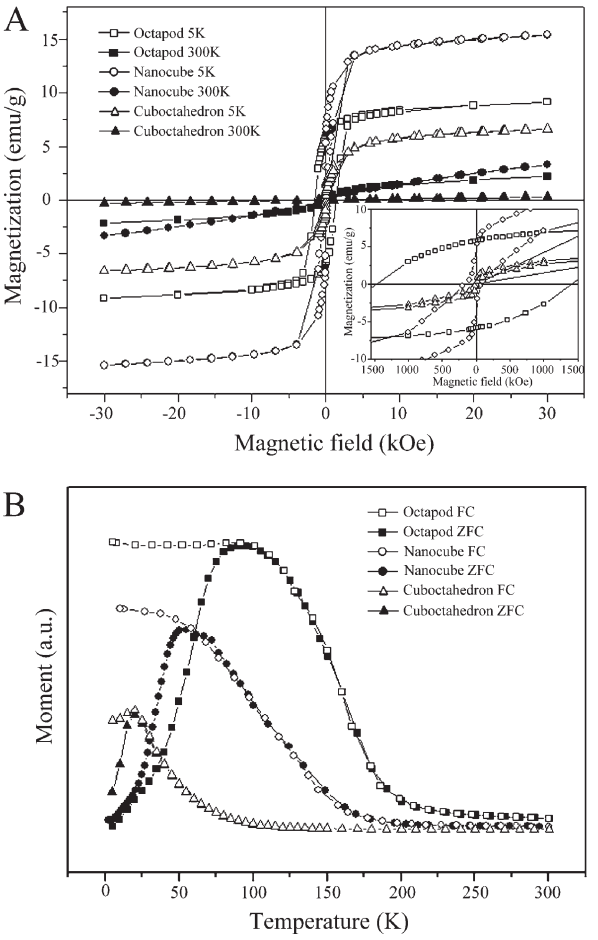

Figure 7. (A) Measurement of magnetization verse magnetic field for octapod, nanocube and cuboctahedron at 5 and 300 K. The inset is an enlargement of the low field part of measurements at 5 K. (B) The measurement of magnetization verse temperature, including zero-field cooling (ZFC) and field cooling (FC) for octapod, nanocube, and cuboctahedron at 100 Oe.

The size and shape dependencies of the magnetic properties of cuboctahedrons, octapods and nanocubes (Fe/Pt = 72/28) were investigated. Figure 7A shows their hysteresis loops at 5 and 300 K. All three samples exhibit the superparamagnetic behavior at 300K. The saturated magnetization (M_s) at 5 and 300 K are in the sequence: $M_{s\ (\text{nanocube})} > M_{s\ (\text{octapod})} > M_{s\ (\text{cuboctahedron})}$ and the coercivity of octapod (1461 Oe), nanocube (164 Oe) and cuboctahedron (11 Oe) are also obtained. The blocking temperature as observed in Figure 7B is 20, 50, and 95 K for cuboctahedrons, nanocubes and octapods, respectively. Several studies have indicated that M_s, coercivity, and blocking temperature of magnetic nanocrystals were proportionally responsible for their

(36) Xia, Y.; Xiong, Y.; Lim, B.; Skrabalak, S. E. *Angew. Chem., Int. Ed.* **2009**, *48*, 60.
(37) Zu, L. J.; Norris, D. J.; Kennedy, T. A.; Erwin, S. C.; Efros, A. L. *Nano Lett*. **2006**, *6*, 334.

volumes.[38,39] In our case, the order of volume (V) based on TEM measurements, $V_{(\text{nanocube})} > V_{(\text{octapod})} > V_{(\text{cuboctahedron})}$, obviously reflects the order of M_s. Also, as we expected, cuboctahedrons exhibit the lowest coercivity and blocking temperature among all the nanocrystals. However, the coercivity and blocking temperature (T_b) of nanocubes are lower than those of octapods, which cannot be simply explained by their volume difference.

The difference of the coercivity between octapod and nanocube can be understood by their shape differences. Previous studies have demonstrated that coercivity increased with the increase of the effective magnetocrystalline anisotropy constant, K_{eff}.[40] A simple equation, $K_{\text{eff}} = K_B + 6K_S/d$, is used to account for the K_{eff} difference between octapods and nanocubes, where K_B is the bulk magnetocrystalline anisotropy constant, K_S is the surface anisotropy constant, and d is the diameter of nanocrystals.[41] On the basis of our experimental results in Figure 7A, we expect that K_{eff} of octapods is higher than that of nanocubes because the coercivity of octapods is higher. Here, $d_{(\text{nanocube})}$ is close to $d_{(\text{octapod})}$ and therefore $K_{S(\text{octapod})}$ is higher than $K_{S(\text{nanocube})}$. In comparison to the $K_{S(\text{nanocube})}$, the higher $K_{S(\text{octapod})}$ is attributed to its higher surface to volume ratio and more structural facets.[11,42−44] To further understand the result of $T_{b(\text{octapod})} > T_{b(\text{nanocube})}$, the formula $T_b = K_{\text{eff}}V/25k_b$ is used to estimate T_b, where k_b is Boltzmann's constant and V is the volume of a single FePt nanocrystal.[45] Although the $V_{(\text{octapod})}$ is slightly smaller than $V_{(\text{nanocube})}$, the different K_{eff} values between both samples imply that $T_{b(\text{octapod})}$ is larger than $T_{b(\text{nanocube})}$. The results agreed with the measurements as shown in Figure 7B.

Conclusion

In conclusion, The FePt nanocrystals with octapod, cuboctahedral, truncated cubic, and cubic shapes were successfully prepared in a solution reaction. The proposed growth model provided a new conception for shape-controlled growth of alloy magnetic nanocrystals. The magnetic measurements of FePt octapod and nanocubes showed the remarkable shape dependencies on their magnetizm. The syntheses of other types of alloy magnetic nanocrystals are in progress.

Acknowledgment. This work was supported by NSC, TNSTPNN, IAMS, and NTNU. We are also very grateful to Dr. Chung-Li Dong for the discussion on magnetic property of FePt nanocrystals.

(38) Shevchenko, E. V.; Talapin, D. V.; Schnablegger, H.; Kornowski, A.; Festin, O.; Svedlindh, P.; Haase, M.; Weller, H. *J. Am. Chem. Soc.* **2003**, *125*, 9090.
(39) Park, J.; Lee, E.; Hwang, N. M.; Kang, M. S.; Kim, S. C.; Hwang, Y.; Park, J. G.; Noh, H. J.; Kini, J. Y.; Park, J. H.; Hyeon, T. *Angew. Chem., Int. Ed.* **2005**, *44*, 2872.
(40) Chikazumi, S. *Physics of Ferromagnetism*; Clarendon: Oxford, U.K., 1997.
(41) Bødker, F.; Morup, S.; Linderoth, S. *Phys. Rev. Lett.* **1994**, *72*, 282.
(42) Jamet, M.; Wernsdorfer, W.; Thirion, C.; Dupuis, V.; Melinon, P.; Perez, A.; Mailly, D. *Phys. Rev. B* **2004**, *69*, 024401–1.
(43) Cheng, R.; Bader, S. D.; Fradin, F. Y. *Phys. Rev. B* **2008**, *77*, 024404–1.
(44) Cozzoli, P. D.; Snoeck, E.; Garcia, M. A.; Giannini, C.; Guagliardi, A.; Cervellino, A.; Gozzo, F.; Hernando, A.; Achterhold, K.; Ciobanu, N.; Parak, F. G.; Cingolani, R.; Manna, L. *Nano Lett.* **2006**, *6*, 1966.
(45) Cullity, B. D. *Introduction to Magnetic Materials*; Addison-Wiley: Reading, MA, 1972.